

## STRUCTURAL, MORPHOLOGICAL AND PHOTOCATALYTIC PROPERTIES OF Co DOPED ZnO NANOPARTICLES

M. S. PRATHAP REDDY<sup>a</sup>, P. T. POOJITHA<sup>b</sup>, V. K. M. SMITHA RANI<sup>b</sup>,  
M. KUMAR<sup>c\*</sup>

<sup>a</sup>*School of Electronics Engineering, Kyungpook National University, Daegu 41566, South Korea*

<sup>b</sup>*Siddhartha Educational Academy Group of Institutions, Tirupati-517505, A.P. India.*

<sup>c</sup>*Department of Electronic Engineering, Yeungnam University, Gyeongsan 38541, South Korea*

In this work we fabricated ZnO nanoparticles with Co (0- 4 at%) doping and achieved tunable properties. The shift in the X-ray diffraction patterns confirmed the successful doping of Co<sup>2+</sup> ions into the ZnO matrix. The morphological study of the ZnO:Co samples from the results of low- resolution transmission electron microscopy shows the presence of typical hexagonal-shaped particles. Alteration in the intensity of the E<sub>2</sub> (high) mode gives a sufficient evidence for the presence of intrinsic defects related to the oxygen atoms. Diffuse reflectance spectroscopy (DRS) measurements provide promising proof to alter the optical band gap of ZnO nanoparticles via Co doping, with a typical red shift due to sp-d exchange interaction. The Co doped samples displayed a higher photocatalytic activity, during the degradation of Congo red (CR) dye under UV-light illumination compared with the pure ZnO samples. The enhanced photocatalytic activity of the ZnO:Co nanoparticles may be ascribed to the increased oxygen defects induced by the Co substitution in the ZnO host crystal lattice.

(Received November 23, 2017; Accepted January 16, 2018)

*Keywords:* ZnO; Transmission electron microscopy; Photocatalysis

### 1. Introduction

Nowadays, the advancement in nanocrystalline ZnO-based research has been swift, leadings to significant progress in the fundamental sciences and modern technologies [1]. Doping of these materials is an essential and an effective path for enhancing the optical and the magnetic properties of semiconductors, thereby increasing their applicability [2-4]. In particular, doping of transition metals (TM) into the ZnO host lattice enhances the optical absorption, which influences the optical bandgap, making it suitable for photocatalytic applications. However, the selection of a dopant is crucial for a successful doping. The difference in the ionic radii between the dopant and the host cation should be close. Hence, we have chosen cobalt as the dopant for the present investigation. Since, the ionic radius of the cobalt (0.72 Å) is very close to that of the divalent Zn (0.74 Å), it can easily replace the Zn ions in the ZnO lattice. In addition, very few attempts have been made to study the photocatalytic properties of ZnO:Co nanostructures [5–8] and with divergent results. Hence, the photocatalytic properties of the ZnO:Co nanoparticles (NPs) are unclear. The aim is to make an attempt to investigate the photocatalytic properties of the ZnO:Co NPs in the current study. In the present study, we used the co-precipitation method to synthesize ZnO:Co (0, 2, and 4 at%) NPs and analyzed their structural, morphological, optical, and photocatalytic properties. We strongly anticipate that, the present investigation will be very useful to understand the photocatalytic properties of the ZnO:Co NPs.

---

\*Corresponding author: mkshekhawat22@gmail.com

## 2. Experimental

Chemical co-precipitation is the most economical and successful method for the synthesis of the ZnO:Co (0, 2 and 4 at%) NPs. For the preparation of ZnO:Co (0, 2, and 4 at%) NPs, 0.2 M zinc acetate solution (50 ml) was mixed in varying concentrations of cobalt nitrate solution (0–4 at%) with constant stirring. Then, 0.2 M of KOH solution (50 ml) was added drop wise to the above mixture. Finally, 1 ml of polyethyaleyneglycol (PEG) was added to the mixture to stabilize the surface of the nanoparticles. The mixture was then stirred at 70°C for 24 h. The precipitate was rinsed four times with absolute ethanol as well as deionized water to extract the impurities and then dried at 400°C for 4 h.

The samples were subjected to X-ray diffraction (XRD) (Seifert, 3003- TT) with 1.5406 Å Cu-K $\alpha$  radiation) to analyze their phase purities and crystal structures. The morphologies and crystallite sizes of the samples were analyzed using transmission electron microscopy (TEM, FEI, Tecnai-12). Diffuse reflectance spectroscopy (DRS), measurement was recorded using a UV-Vis-NIR double beam spectrophotometer (Cary, 5000). The photocatalytic degradation of CR was performed under UV light radiation using a 16 W UV lamp with a wavelength of 254 nm. 100 mg of the ZnO:Co (0-4 at%) NP catalysts and 100 ml of the CR solution were mixed in a reactor. This solution was stirred at 20°C in the dark for 60 min to obtain an equilibrium mixture., At an interval of 20 min, 5 ml of the reaction mixture was collected with a syringe and was immediately centrifuged to detect the effect of the CR adsorption on the catalyst. The UV lamp was turned on after which 4 ml of the reaction mixture was collected at a 40-min interval. The collected solutions were analyzed with UV-Vis-NIR (Cary, 5000) spectrophotometer.

## 3. Results and discussions

### 3.1. XRD analysis

The structure and phase purity of the ZnO:Co (0, 2 and 4 at%) NPs was confirmed using XRD. Fig. 1 displays the XRD patterns of the ZnO NPs with different doping concentrations of cobalt. The patterns indicate polycrystallinity of the synthesized samples. The XRD patterns of these samples are in good agreement with the JCPDS (No. 36-1451), standard data of hexagonal ZnO powder.

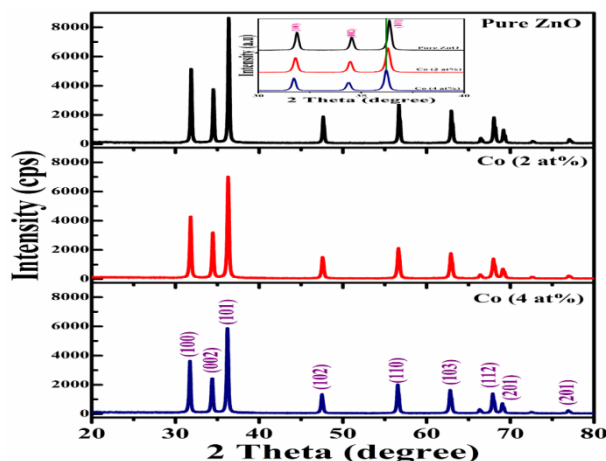


Fig. 1 XRD patterns of the ZnO:Co (0, 2 and 4 at.%) nanoparticles

The influence of Co doping into ZnO is evident from the moderate shift of the (101) peak to a lower angle with increasing Co doping. This shift of the XRD peaks indicates that Co doping in the ZnO lattice is successful. The high resolution XRD peak shift of the (101) peak is also displayed in the inset of Fig. 1. A small variation in the lattice parameters was noticed, however,

the hexagonal phase remains the same. It is not affected by the doping of cobalt into the host lattice at least up to the detection level of the instrument. Moreover, the incorporation of Co into the ZnO lattice is evident from the absence of foreign phases related to either cobalt cluster or cobalt oxides. The average crystallite sizes  $D$  of the ZnO:Co samples were calculated using the Debye–Scherrer equation and they were found to be 19.3 nm, 17.2 nm, and 16.6 nm for the 0, 2, and 4 at% of Co doping, respectively. The decrease in the crystallite sizes of ZnO with an increase in the Co content, suggests that the Co incorporation into the ZnO host lattice gradually decreases the grain growth. A similar result for the cobalt doped ZnO NPs was reported earlier [11, 12]. The estimated lattice constants are as follows:  $a = b = 3.2566 \text{ \AA}$ ,  $c = 5.2088 \text{ \AA}$  for ZnO (pure),  $a = b = 3.2500 \text{ \AA}$ ,  $c = 5.2101 \text{ \AA}$  for ZnO:Co (2 at%), and  $a = b = 3.2496 \text{ \AA}$ ,  $c = 5.2091 \text{ \AA}$  for ZnO:Co (4 at%) NPs.

### 3.2. Morphology studies

Fig. 2 shows the low-resolution TEM images of (a) pure ZnO (b) ZnO:Co (2 at%), and (c) ZnS:Co (4 at%) NPs and these images show that the prepared nanoparticles are distinctly hexagonal and are monodispersed.

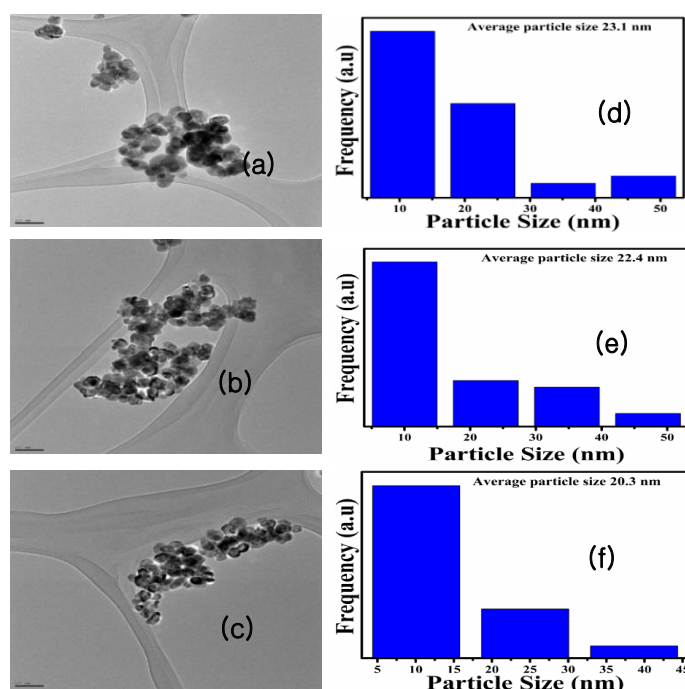


Fig. 2 Low resolution TEM images and size distribution histograms of the (a & d) ZnO, (b & e) ZnO:Co (2 at.%) and (c & f) ZnO:Co (4 at.%) nanoparticles

Figure. 2 (d)-(f) display the average size distribution histograms of the synthesized samples. The estimated particle sizes are found to be 23.1 nm, 22.4 nm, and 20.3 nm for 0, 2, and 4 at% Co ZnO:Co NPs, respectively.

### 3.3. Raman studies

Fig. 3 depicts the RT Raman spectra of ZnO:Co (0, 2, and 4 at%) NPs, overlooked by an intense peak at  $440 \text{ cm}^{-1}$ , corresponding to  $E_2$  (High) mode, which is a common characteristic of the ZnO hexagonal phase.

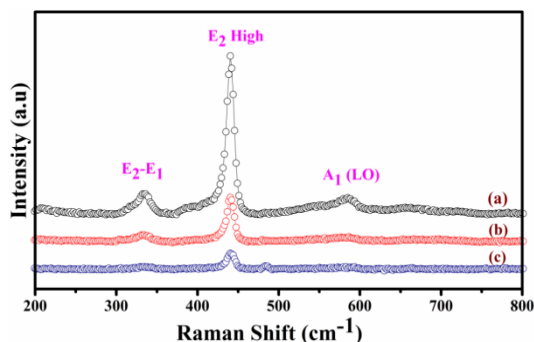


Fig. 3 Raman spectra of (a) ZnO, (b) ZnO:Co (2 at.%) and (c) ZnO:Co (4 at.%) nanoparticles

The intensity of this mode decreases as well as the line width increases with the substitution of Co in the ZnO lattice. This creates a few intrinsic defects related to the oxygen atoms [13] that results in the shift of the peak towards a lower wavenumber. The next peak noticed at  $333\text{ cm}^{-1}$  is assigned to a second order spectral feature originating from the zone boundary phonons of  $2\text{-E}_2\text{ (M)}$  in ZnO. The first-order Raman feature for the prepared samples was recognized at  $586\text{ cm}^{-1}$  assigned to the  $\text{A}_1\text{ (LO)}$  mode that gets diminished after Co doping. The absence of Raman bands between  $470\text{--}550$ ,  $610\text{--}630$ , and  $650\text{--}730\text{ cm}^{-1}$  indicate the absence of  $\text{Co}_3\text{O}_4$  oxide in the prepared samples [14]. The results suggest that the absence of the secondary/impurity phases and ZnO lattice defects could be considered as an essential point for the synthesized nanoparticles to have a single phase and be crystallized homogeneously. Therefore, we believe that the substitution of Co ions that brings lattice disorder as well as defects into the ZnO host, could be the cause for a drastic decrease in the symmetric nature and intensity of the Raman peaks.

### 3.4. DRS studies

To explore the electronic interactions near to the band gap zone due to the Co, DRS measurements were performed for the ZnO:Co (0, 2, and 4 at%) samples in the UV-Vis region as shown in Fig. 7. From these spectra, the Co doped samples display three bands at 565, 609 and 654 nm and are characteristic of d-d transitions in tetrahedrally coordinated divalent (+2) cobalt, which are substituted  $\text{Zn}^{2+}$  ions. Moreover, the absorption edge of the doped samples shifts moderately to (red shift) lower energies wavelength side than that of pure ZnO, indicating a decrement of the band gap as a function of Co doping. The red shift of the doped samples may be attributed to the sp-d exchange interactions among the localized 'd' electrons of the dopant ions and band electrons.

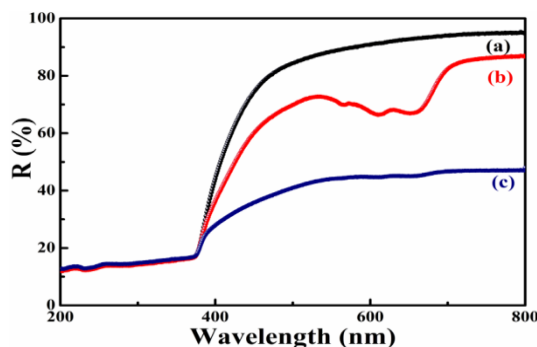


Fig. 4 DRS spectra of (a) ZnO, (b) ZnO:Co (2 at.%) and (c) ZnO:Co (4 at.%) nanoparticles

### 3.5. Photocatalysis studies

Hexagonal Co doped ZnO NPs are estimated to have an improved photocatalytic activity

than that of pure ZnO. We tested the photocatalytic activity of hexagonal Co doped ZnO NPs to investigate their multifunctional applicability. We used the ZnO:Co NPs as sorbents for degradation of CR in a solution under UV radiation. A noticeable decrease in the band gap energy of the Co doped ZnO NPs was observed with increasing Co concentration that motivated us to study the degradation of the common textile dye, CR under UV radiation. Figure. 5 shows the UV-Vis absorption spectra of CR with irradiation time on the ZnO:Co (4 at%) NPs. After 120 min of irradiation, 54.1% of CR was degraded with ZnO:Co (4 at%) NPs.

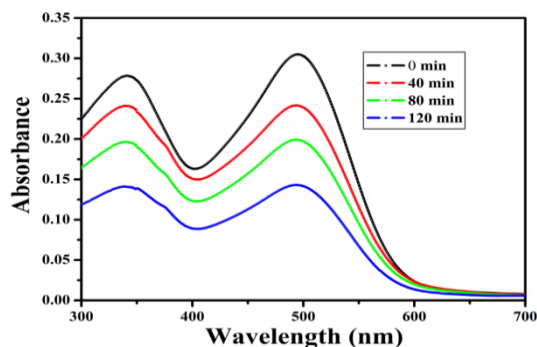


Fig. 5 UV-vis absorption spectra changes of CR aqueous solution in the presence of ZnO:Co (4 at%) nanoparticles

For comparison, the photodegradation of CR in dark and without a catalyst (blank) was also studied. A plot of  $C/C_0$  versus time reveals that the Co doped ZnO NPs were able to degrade the dye faster than the pure ZnO NPs (Fig. 6). In the case of the blank test, negligible photodegradation of CR was observed. Only 31.35% of CR degradation was observed with pure ZnO NPs. The photocatalytic degradation kinetics of the CR solution with ZnO:Co (0, 2, and 4 at%) nanoparticles under UV light irradiation are shown in Fig. 7. The degradation efficiency of CR with ZnO:Co (4 at%) in 120 min under UV radiation is 54.1%. ZnO:Co (4 at%) shows higher photocatalytic activity than ZnO:Co (2 at%) (45.8%) and pure ZnO NPs. The enhanced photocatalytic efficiency of the Co doped ZnO NPs may be due to the increase in oxygen vacancies and defects by cobalt doping.

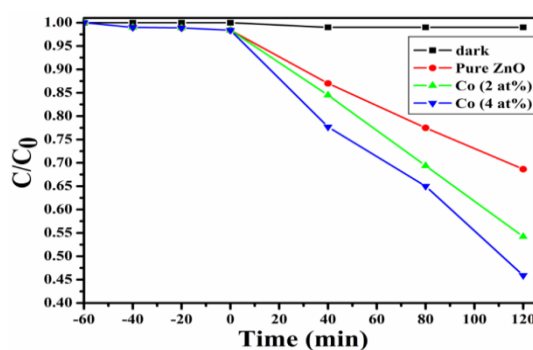


Fig. 6 Photocatalytic activities of ZnO:Co (0, 2 and 4at%) nanoparticles

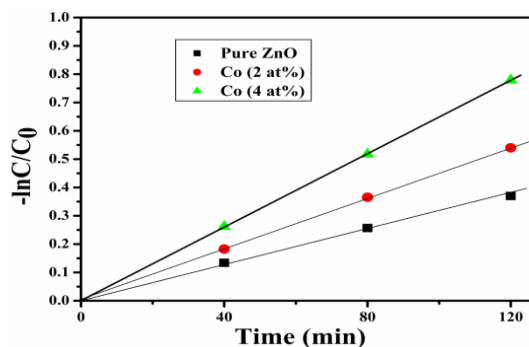


Fig.7 Kinetic linear simulation of CR photocatalytic degradation over the ZnO:Co (0, 2 and 4at%) nanoparticles

These results strongly suggest that the Co doped ZnO NPs are promising candidates for CR dye degradation. Anandan et al. [5] reported that the photocatalytic activity of the Co doped ZnO was less than that of the undoped ZnO for the degradation of methyl green (MG) dye under UV radiation. Recently, Xu et al. [6] reported that the photocatalytic activity of ZnO:Co NPs was better than that of the pure ZnO NPs for the degradation of methyl orange (MO) dye. Manjula et al. [7] observed a decrease in the photocatalytic efficiency of the Co doped ZnO NPs than that of the pure ZnO NPs for the degradation of methyl blue (MB) dye under UV illumination. This is the first report on the degradation of CR dye using Co doped ZnO NPs.

#### 4. Conclusions

ZnO:Co (0, 2, and 4 at%) nanoparticles were synthesized by chemical co-precipitation method. XRD analysis shows that the samples have a hexagonal structure and confirms that the Co ions were successfully substituted in the lattice sites of Zn ions in the ZnO host matrix. Alteration in the intensity of the E<sub>2</sub> (high) mode gives a sufficient evidence for the presence of intrinsic defects related to the oxygen atoms.

DRS spectra display two results as a function of Co concentration, one is red shift and two is three absorption bands (*d-d* transitions), which are both interpreted to be due to the Co entered in the ZnO matrix. The photocatalytic activity of pure and doped ZnO NPs was investigated by studying the degradation of an organic dye as a function of irradiation time. The results indicate that the photocatalytic activity of the doped ZnO NPs was found to be higher than that of the pure ZnO NPs for the degradation of the dye. We believe that the improved photocatalytic activity of the Co doped ZnO nanoparticles may be attributed to the increase in oxygen vacancies and defects caused by cobalt doping.

#### References

- [1] Mohammed M. Rahman, Sher Bahadar Khan, Abdullah M. Asiri, Khalid A. Alamry, Aftab Aslam Parwaz Khan, Anish Khan, Malik Abdul Rub, Naved Azum, *Micro Chim. Acta*, **180**, 675 (2013).
- [2] Gunjan Srinet, Ravindra Kumar, Vivek Sajal, *J. Appl. Phys.* **114**, 033912 (2013).
- [3] Hayoung Yoon, Jun Hua Wu, Ji Hyun Min, Ji Sung Lee, Jae-Seon Ju, Young Keun Kim, *J. Appl. Phys.* **111**, 07B523 (2012).
- [4] B. Poornaprakash, U. Chalapathi, B. Purusottam Reddy, P.T. Poojitha, Si-Hyun Park, *J. Alloy Compd.* **705**, 51 (2017).
- [5] M. Anandan, S. Dinesh, N. Krishnakumar, K. Balamurugan, *Mater. Res. Express* **3**, 115009 (2016).
- [6] Chao Xu, Lixin Cao, Ge Su, Wei Liu, Xiaofei Qu, Yaqin Yu, *J. Alloy Compd.*

- 497**, 373 (2010).
- [7] Manjula G. Nair, M. Nirmala, K. Rekha, A. Anukaliani, *Mater. Lett.* **65**, 1797 (2011).
- [8] Yongchun Lu, Yanhong Lin, Dejun Wang, Lingling Wang, Tengfeng Xie, Tengfei Jiang, *Nano Res.* **4**(11), 1144 (2011).
- [9] J. Hays, K.M. Reddy, N.Y. Graces, M.H. Engelhard, V. Shutthanandan, M. Luo, C. Xu, N.C. Giles, C. Wang, S. Thevuthasan, A. Punnoose, *J. Phys.: Condens. Matter.* **19**, 266203 (2007).
- [10] A. Sivagamasundari, R. Pugaze, S. Chandrasekar, S. Rajagopan, R. Kannan, *Appl Nanosci.* **3**, 383 (2013).
- [11] G. Mohan Kumar, P. Ilanchezhian, Jin Kawakita, M. Subramanian, R. Jayavel, *Cryst Eng Comm* **12**, 1887 (2010).
- [12] Huijuan Zhou, Limei Chen, Vivek Malik, Christoph Knies, Detlev M. Hofmann, Kanwal Preet Bhatti, S. Chaudhary, Peter J. Klar, Wolfram Heimbrod, Claus Klingshirn, Heinz Kalt, *phys. stat. sol. (a)* **204** (1), 112 (2007).